INCORPORATING SCENE CONSTRAINTS INTO THE TRIANGULATION OF AIRBORNE OBLIQUE IMAGES

M. Gerke and A.P. Nyaruhuma

International Institute for Geo-Information Science and Earth Observation – ITC, Department of Earth Observation Science, Hengelosestraat 99, P.O. Box 6, 7500AA Enschede, The Netherlands, {gerke,nyaruhuma09656}@itc.nl

KEY WORDS: Adjustment, Bundle, Calibration, Comparison, Orientation, Software

ABSTRACT:

An increasing number of airborne systems equipped with oblique viewing cameras are reported being operational, such as Pictometry, FLI-MAP, 3K or PFIFF. The oblique images are today mainly used for visualization purposes, but they are also interesting for instance for cadastre applications.
In order to optimize the exterior orientation, and eventually also to calibrate the interior orientation and distortion parameters, it is a common means in close-range photogrammetry related literature to incorporate scene constraints into the block adjustment. As oblique airborne cameras image vertical man made structures like building façades, it becomes possible to introduce strong geometric constraints also here. Examples are horizontal and vertical line features at façades and the rectangular alignment of these features.
In this paper we introduce our own approach to airborne image triangulation, where the mentioned constraints are explicitly exploited in the block adjustment of images from multiple camera devices, including self-calibration. The influence of the scene constraints is validated by comparing the results from our approach to results obtained from the commercial software packages LPS 9.2, ImageModeler 2009, and Boujou 4.1. All these systems have different properties with respect to the incorporation of scene constraints and options for self-calibration.
A data set of oblique and vertical images from a FLI-MAP 400 (Fugro Aerial Mapping B.V.) flight over Enschede is used for the experiments. The experiments reveal that the easily definable scene constraints enhance the overall result of bundle block adjustment and self-calibration. Due to the restricted self-calibration capabilities for multiple camera set-ups the results from LPS are not optimal. In addition, it is not possible to incorporate scene constraints into LPS. In contrast, ImageModeler and Boujou are focussing on the use of uncalibrated consumer cameras and show also more options with respect to the use of constraints. All types of constraints can be incorporated only in our own approach and at the same time our method allows the self-calibration of multiple devices. Because of those reasons our method resulted in the best overall solution.

1 INTRODUCTION AND RELATED WORK

An increasing number of airborne image acquisition systems are operational (Petrie and Walker, 2007). Because of the availability of low-cost digital cameras with small or medium sized sensors, some of those systems carry multiple cameras covering different viewing directions. Examples are: Pictometry, FLI-MAP or MIDAS. For instance Pictometry data is available already for a number of cities and they are accessible in the category "birds eye view" in Microsoft Virtual Earth.

Compared to vertical airborne images, the oblique images have some specific properties. Depending on the tilt angle, the scale within the images varies considerably. Moreover, vertical structures of raised objects like buildings or trees are imaged, but the (self)occlusion by those objects is much more significant compared to the vertical image case.

The use of oblique images for topographic mapping purposes was shown in quite some papers. In (Höhle, 2008) height determination from single oblique images is demonstrated. The verification of vector data using oblique imagery is shown in (Mishra et al., 2008). Due to the fact that building façades are well visible in oblique images, some researchers concentrate on how to automatically extract façade textures (Früh et al., 2004, Wang et al., 2008). Besides, the oblique images are interesting for cadastre applications, because the building outline as defined at the vertical wall is directly visible (Lemmen et al., 2007).

Concerning the calibration and orientation of the image sensors, it is a common means to calibrate intrinsic camera parameters beforehand in the lab and perform direct or integrated sensor orientation through the use of GPS/IMU devices (Kurz et al., 2007, Grenzdörffer et al., 2008). However, the classical indirect sensor orientation by bundle block adjustment, possibly including self-calibration, is not dispensable, because of the following reasons: a high quality and thus expensive GPS/IMU unit may not be available, for instance on an unmanned airborne vehicle (UAV); the cameras are not rigidly mounted on the airborne platform; the cameras are not (thoroughly) calibrated beforehand, or the calibration information is not reliable.

For a bundle block adjustment it is necessary to have sufficient geometric control information. Classically these are ground control points (GCPs), being well distributed in the target area. In close-range application it is also common to incorporate constraints from the scene directly, such as straight lines, planes etc., c.f. (Luhmann et al., 2006). Since airborne oblique images may sufficiently cover vertical man-made structures like building façades, it becomes possible to incorporate constraints from them into the adjustment, such as horizontal or vertically aligned window edges, or the right angle represented by those features. Such an integration would have several advantages: Given that the scene constraints comply with the orientation of the coordinate system planes defined by the GCPs, they might contribute to a further stabilization of the block, with a possible consequence that the number of GCPs can be reduced. In the most ideal case GCPs are then only necessary for the datum definition, i.e. the absolute orientation of the block. This is interesting as the acquisition of GCPs might be very laborious and expensive. For some applications, like image-based modeling, the absolute orientation of an image block with respect to a pre-defined datum is not always interesting. However, it is very helpful if a local coordinate system is defined in compliance with the building geometry, i.e. the x-y-plane represents the horizontal plane. If this is given, the object modeling and reconstruction from the images

can be constrained with respect to the local coordinate system. For such applications, the incorporation of the described scene constraints will impose a strong geometry and at the same time define implicitely an appropriate coordinate system.

The effect of using scene constraints and GCPs in the adjustment is depicted in Fig. 1: The upper drawing shows the profile along the horizontal plane of an area, covered by airborne images. If GCPs are not used, they will not be connected to the optimal plane and horizontal and vertical lines will be tilted in the model. However, if the GCPs and horizontal and vertical lines are used to constrain the geometry, the final plane will be a better approximation of the optimal one, and the horizontal and vertical features will be aligned accordingly.

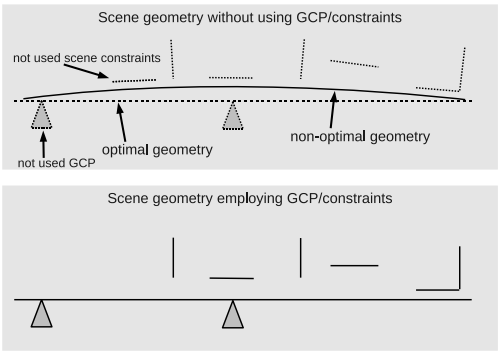

Figure 1: Effect on the geometry if scene constraints are incorporated. Upper: without using GCPs or constraints, Lower: employing GCPs/constraints

In this paper we present our own approach to airborne image triangulation, where the scene constraints *horizontal line*, *vertical line* and *right angle*, are explicitly introduced in the block adjustment of images from multiple camera devices, including self-calibration.

Only little similar was found in the literature. In (Früh et al., 2004) a method to orient oblique airborne images using existing 3D building models is introduced. Lines from the 3D model are matched with edges extracted from the images and then the extrinsic image orientation and the focal length are adjusted by minimizing the reprojection error of the 3D lines, as defined by their endpoints. The final application is then to extract textures from the image to be pasted onto the model. This is a fully automatic approach, but the images are only oriented with respect to a generalized and possibly out-dated or inaccurate building model. In (Wang et al., 2008) a similar approach to the former one is described, but instead of minimizing the reprojection error the authors directly incorporate the coplanarity equation into the adjustment. By this means they only match line segments and do not need to care for correctly matched line endpoints. Unfortunately, no detailled evaluation of this approach is presented in the paper.

In the following we will describe our approach to incorporate scene constraints into the bundle block adjustment of airborne images. Our method will be compared to the approaches implemented in three commercially available software packages which are: Boujou 4.1 (by 3d2), ImageModeler 2009 (by Autodesk), and LPS 9.2 (by Erdas). In section 3 we report about experiments which have been conducted to evaluate the quality of our approach, also versus the three other software packages. The usefulness of the approach is tested also in the framework of a free net adjustment. Finally, section 4 concludes this paper and gives a brief outlook to further work.

2 INTEGRATING SCENE CONSTRAINTS INTO BLOCK ADJUSTMENT

Scene constraints applied Scene constraints are integrated in two different ways. One is to define the endpoints of a line and require them to be aligned *horizontally* or *vertically*. This means, their z-component must be identical, or their projection into the x-y-plane must be the identical point, respectively. The constraint *right angle* is realized through the three corner points of a triangle, where the angle at the center point needs to be equal to 90°.

All three constraint types can be found naturally at façades. However, they are not necessarily independent, so for instance if one chooses vertically and horizontally aligned window edges to define the two constraints *horizontal* and *vertical* line the constraint *right angle* does not bring new information in case the former lines have one point in common. However, often one can observe the ridges of a (flat)roof, and assume that they are aligning horizontally and inclosing a right angle. Examples for scene constraints are shown in Fig. 2. The long façade at the shopping center and the tower forming horizontal and vertical lines, respectively. The right angle at the tower contributes to the constraint right angle, but in addition can be used for a horizontal or vertical line constraint. Alternatively one could define a horizontal and a vertical line constraint in that case.

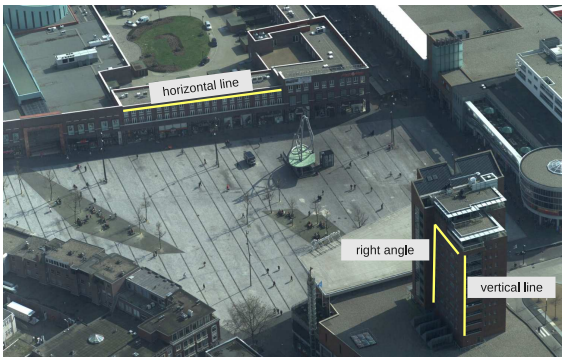

Figure 2: Examples for the three different constraint types

Integration into adjustment In our approach we apply the standard Gauss-Markov adjustment method, i.e. we define the observations L, in this case image coordinates, as functions from the unknowns X: $L_i = F_i(X)$ (collinearity). The unknowns are the exterior orientation for each image and the coordinates of the tie points in object space. For self-calibration the unknowns are extended with interior orientation and lens distortion parameters.

The scene constraints as well as ground control points are integrated into the adjustment by formulating so-called "fictive observations" (Niemeier, 2002), i.e. as soft constraints. The idea is that the points being used to define the constraints are unknowns, and the constraints impose a certain geometry on them. One other possibility would be to formulate hard constraints, i.e. to explicitly define a functional relation between the observations and the unknowns (Gauss-Helmert model). The advantage of using soft constraints is that a flexible weighting of the constraints is possible through the stochastic model and in addition the significance of the constraints can be statistically tested after adjustment.

For a *horizontal line* constraint it is requested that after adjustment the two corresponding end points of the line have the same z-coordinate. The *vertical line* constraint is considered in a similar manner, only here the difference between the respective points in x-y-plane need to be minimized. For the *right angle* constraint it is desired that the points defining the triangle satisfy the Pythagorean theorem. For every constraint a fictive observation

is introduced with a high weight in the stochastic model, forcing the unknown points to satisfy the condition.

Overall workflow The workflow as realized within our method is as follows:

1. Reading the approximations for the unknowns: As we apply the Gauss-Markov adjustment method we need sufficiently approximated values for the unknowns in order to perform the linearization. Concerning the interior camera parameters and lens distortion, the approach is quite flexible: it allows to define multiple camera devices, where calibration information might be given or not per device.

2. Robust tie point matching: Sift matches are established in several combinations to increase the reliability. We do matches in all combinations of images, satisfying a minimal overlapping constraint. However, a match is only accepted if the frame-to-frame linking chain confirms the match, c.f. (Gerke, 2008). In the bundle block adjustment all confirmed matched image points contribute observations for a tie point.

3. Reading manually measured tie points, GCP information and constraint definitions.

4. Optimize point number and distribution: For computational reasons it is desired to restrict the total number of observations. Given a pre-defined maximum number of observations, and the minimum number of rays per tie point, the algorithm removes original observations if necessary, where the priority is on preserving a good distribution of points in the particular images. Manually added tie points and points connected to constraints have an even higher priority to ensure that they will not be removed.

5. Least squares bundle adjustment: The adjustment method is applied, whereas the constraints are incorporated as fictive observations, refer to the previous paragraph.

2.1 Comparison with commercial approaches

We now compare our approach to commercial solutions. The adjustment of airborne oblique images can be done in principal by several existing packages. Three categories might be defined for that: A) software from video sequence analysis, applying shape from motion methods to calibrate and orient camera shots, B) software specialized on close-range photogrammetric solutions, mostly coming with image-based modeling capabilities, and finally C) traditional digital photogrammetric workstations. Because of the different application areas those software might already be able to use scene constraints as defined in this paper. Here, 3 typical software packages are chosen to compare the respective capabilities with our approach: Boujou4.1 by 2d3 (cat. A), ImageModeler 2009 by Autodesk (cat. B) and Leica Photogrammetry Suite 9.2 by Erdas (cat. C). Different criteria are defined to ease the comparison, refer to Table 1, where our approach is given in the last column as *ITC*. Some criteria are of special interest:

- Ground control information: only in LPS and ITC approach one can differentiate between full, plane or vertical GCPs, whereas in LPS it is not possible to explicitly introduce a known distance to support the estimation of the scale.

- Scene constraints: In Boujou it is possible to incorporate scene constraints, but only with respect to the coordinate axes, so *vertical line* is possible, because it is aligned parallel to the z-axis, but *horizontal line* can seldomly be used as the objects in a built-up area are normally not exactly oriented along the axes as defined by a certain datum/map projection. In ImageModeler only *right angles* can be incorporated. In LPS scene constraints can not be incorporated at all.

- The self-calibration is an interesting issue as well, given that multiple camera devices are used. In Boujou the principal point offset and the lens distortion can only be given or estimated for all devices globally, whereas the principal distance can be estimated per image or device. ImageModeler as well as the ITC approach are more flexible as they allow to fix or adjust the IO parameters and distortion per device or image. LPS can perform a sophisticated self-calibration incorporating several distortion models, but only for a setup, where one single camera device is used. This has as a consequence that in a multi-device setup self-calibration is not possible at all in LPS.

3 EXPERIMENTS

The experiments pursue two goals: firstly, the four different approaches as described in the last section are tested with respect to their performance for the adjustment of a small block of airborne imagery, containing both nadir and oblique images. Secondly the ITC approach is analyzed concerning the use of scene constraints in a free net adjustment.

3.1 Description of used data

The data used for these experiments was acquired by the Fugro FLI-MAP-400 system in March 2007 over Enschede, The Netherlands. Besides two LIDAR devices and two video cameras, the system carries two small frame cameras, one pointing vertical, and one oblique camera, looking in flight direction, tilted by approx. 45°. Calibration information (IO parameters and distortions) is available only for the vertical camera. A small block of 7 vertical and 8 oblique images was chosen for the experiments. Unfortunately, the sidelap is very small, partly below 10%, and thus not useful for block adjustment, therefore only one strip was used. In Fig. 3, upper part some parameters of the images are given, in the lower part the layout of the block is shown, including GCP, check points and the approximate position of defined scene constraints.

Parameter	vertical	oblique
flying height [m]	275	275
forward overlap	70%	70%
focal length [mm]	35	105
pixel size [μm]	9	9
sensor size [mm x mm]	36x24	36x24
ground sampling distance [cm] (for oblique: from fore- to background)	7	2.8 – 4

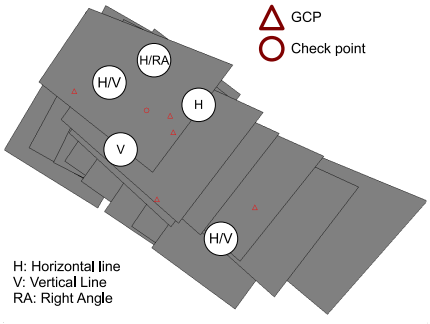

Figure 3: Layout of sample block

Criterion	Boujou	ImageModeler	LPS	ITC
Needs approximation of unknowns	no	no	yes	yes
Automatic tie point measurement	yes (feat. tracking)	no	yes (cc)	yes (sift)
Blunder detection	yes	no	yes	yes
Use of multiple cameras	yes	yes	yes	yes
Self calibration: Principal point single/multiple cameras	yes/no	yes/yes	yes/no	yes/yes
Self calibration: Principal distance single/multiple cameras	yes/yes	yes/yes	yes/no	yes/yes
Self calibration: Lens distortion single/multiple cameras	radial yes/no	radial yes/yes	several models yes/no	radial,tangential yes/yes
Adjustment: Ground control info	full GCP, known distance	full GCP, known distance	full, plane, height GCP	full, plane, height GCP, known distance
Adjustment: Scene constraints	plane (line) parallel to coordinate plane (axis)	right angle	none	plane parallel to coordinate plane, vertical/horizontal line, right angle

Table 1: Comparison of approaches

3.2 Performance of the four approaches

Tested setups Different set-ups have been defined to test the influence of the scene constraints on the block adjustment:

- only oblique, no constraints `(I-A)`: here, only the oblique images were used, and no constraints were defined [done in all software solutions],
- only oblique, with constraints `(II-A)`: again, only the oblique images were used, but the constraints are enabled [not for LPS as not constraints possible],
- all images, with constraints `(II-B)`: now, also the vertical images were used in addition [in LPS: no constraints `(II-A)`, in all other software solutions the constraints are used and IO parameters, including distortions are estimated. For ITC also the calibration information as provided by Fugro was used in a separate test `(II-B(f))`].

The GCPs and check point coordinates were obtained with a RTK-GPS equipment. To assess the accuracy of the adjustment, the RMSE at GCPs, at check points and at the scene constraints is computed, where some scene constraints are used as check constraints. But note that for the right angle-constraint the RMSE is derived from the difference of the adjusted value to 90°.

Results and interpretation In the following the RMSE values are given per software solution, both as tables and diagram. In the very end of this section we give a brief overall interpretation. The results from Boujou are shown in Fig. 4. In the oblique images the check points were occluded by buildings, only the height of a height control point is used as check information, because height GCPs can not be used in Boujou. In general, the residuals are quite large: around 1m at the GCPs and 50cm at the height check point. The difference at the horizontal line checks is about 40cm, and 1m at the vertical check features. The angle RMSE is about 6°. After including all images and using the vertical constraint, which is the only possible one in Boujou, the X-Y component of the RMSE at the control points is reduced considerably to less than 15cm, however the height component is worse than in the first setup. It seems that the constraint has no influence on the result, because the RMSE at the vertical constraint and check features does not decrease in total. Also the values with respect to the angles do not improve. Setup `(II-A)` where only the oblique images and constraints were used is not listed, because it showed no difference at all to the setup without constraints, so the constraints had no effect on the adjustment.

Several circumstances may cause those results. The overall approach in Boujou to incorporate GCP is the following: in an image where at least 4 GCPs are visible, the image orientation

Assessment	I-A	II-B
X-Res. at GCP	0.907	0.146
Y-Res. at GCP	1.176	0.128
Z-Res. at GCP	0.801	1.012
X-Res. at Check		0.064
Y-Res. at Check		0.034
Z-Res. at Check	0.422	1.200
Res. at H-check	0.397	0.298
Res. at V-constraints		1.401
Res. at V-check	1.107	0.195
Res. at RA-check (rad)	0.115	0.097
Res. at RA-check (°)	6.568	5.545

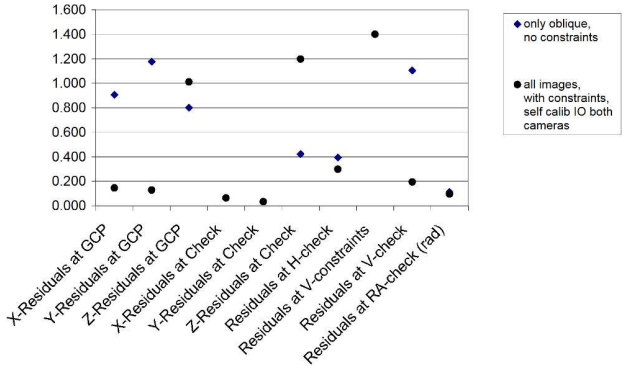

Figure 4: Results Boujou

is computed, including an estimation of the focal length. No documentation about the algorithm is available, but it can be assumed that a spatial resection is applied, including an estimation of the focal length. After this has been done for all the images with enough GCPs, the remaining images are connected to the initial ones by a bundle block adjustment, employing also the tie points as measured by an operator or through feature tracking. In order to avoid extrapolation, the first and the last image of the sequence need to be estimated directly through control points. In the case at hand we had not enough GCPs for the first and last image, so we took some tie points from the LPS project after adjustment therein as approximate GCPs. After the described direct computation of the exterior orientation parameters, those approximate GCPs have been removed again. Now it seems that this removal led to some problems. Another problem concerns the radial distortion. This one is considerably large for the vertical camera (up to 30 pixels at the image border), for the oblique camera it is much smaller. However, in Boujou only one radial distortion for the whole project, i.e. for all cameras in common can be defined or estimated. Thus, the errors arising from the lens distortion can not be compensated adequately.

The results from ImageModeler 2009 are shown in Fig. 5[1]. Looking at the diagram one can observe that in general the results from

[1] Note scale difference between this and the former diagram

the first setup are worse than the results from the second setup, and that finally the last setup, where all images and the constraints are used, resulted in even smaller RMSE values. The right-angle constraint seems to have quite a large influence on the calibration, as the RMSE from setup `I-A` to `II-A` decreases for nearly all check values. When the vertical images are added, the RMSE values decrease even more.

Assessment	I-A	II-A	II-B
X-Res. at GCP	0.298	0.219	0.053
Y-Res. at GCP	0.234	0.184	0.061
Z-Res. at GCP	0.178	0.121	0.033
X-Res. at Check			0.144
Y-Res. at Check			0.054
Z-Res. at Check			0.087
Res. at H-constraints			
Res. at H-check	0.323	0.220	0.139
Res. at V-constraints			
Res. at V-check	0.235	0.328	0.235
Res. at RA-constraints		0.097	0.118
Res. at RA-check (rad)	0.067	0.044	0.058
Res. at RA-check (°)	3.852	2.525	3.347

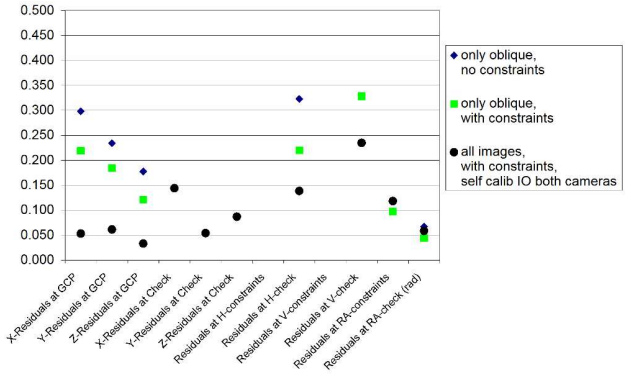

Figure 5: Results ImageModeler

Assessment	I-A	II-A
X-Res. at GCP	0.081	0.037
Y-Res. at GCP	0.053	0.013
Z-Res. at GCP	0.040	0.046
X-Res. at Check		0.174
Y-Res. at Check		0.088
Z-Res. at Check		0.045
Res. at H-check	0.336	0.339
Res. at V-check	0.092	0.219
Res. at RA-check (rad)	0.067	0.076
Res. at RA-check (°)	3.866	4.337

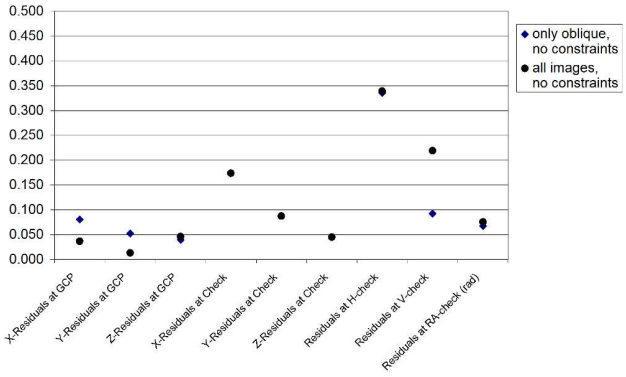

Figure 6: Results LPS

The results from LPS are shown in Fig. 6. For the first setup a self-calibration was performed, as only the oblique looking camera device was incorporated. The results are reasonable, also because the height GCP can be incorporated into the adjustment. As this GCP was on the roof of a very tall building it provides a strong geometry for the self-calibration. For the second setup where the vertical images are added, the IO parameters from the previous self-calibration were fixed for the oblique images and the IO parameters for the vertical images are taken from the calibration protocol. The RMSE values are decreasing considerably, only the residuals in x-direction for the check point are quite large.

The residual at the vertical check constraints are larger compared to the first setup. As the residual from the vertical constraint is directly related to errors in the x-y-plane, the reason behind this observation might be the same as for the increased residual at the check point in x-direction. One explanation for this can again be sought for in the distortions. Although the calibrated values are used for the vertical camera, no distortions for the oblique camera can be defined. Moreover, when looking at the results from the ITC approach, see below, it can be concluded that the calibration parameters as shipped with the data are not optimal.

Assessment	I-A	II-A	II-B(f)	II-B
X-Res. at GCP	0.026	0.030	0.047	0.096
Y-Res. at GCP	0.054	0.070	0.067	0.076
Z-Res. at GCP	0.011	0.034	0.099	0.046
X-Res. at Check			0.105	0.042
Y-Res. at Check			0.007	0.001
Z-Res. at Check			0.090	0.018
Res. at H-constraints		0.007	0.075	0.048
Res. at H-check	0.463	0.139	0.129	0.126
Res. at V-constraints		0.103	0.068	0.067
Res. at V-check	0.394	0.136	0.124	0.038
Res. at RA-constraints		0.028	0.012	0.016
Res. at RA-check (rad)	0.077	0.057	0.062	0.065
Res. at RA-check (°)	4.402	3.292	3.546	3.700

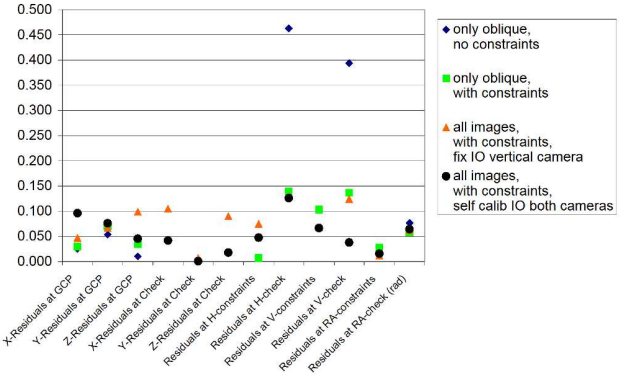

Figure 7: Results ITC approach

Finally, the results from the ITC approach are shown in Fig. 7. The effect of the scene constraints is already obvious from the first to the second setup, i.e. only oblique images without and with employed scene constraints. The residuals at control points only increase marginally, however, the residuals at the scene constraints and the check features decrease considerably: from around 40 to 14cm. In the third setup the vertical images were added, but the IO and distortion parameters were fixed to the values as given from the data supplier. Although it should be expected that those additional images contribute to a better intersection geometry, there is no significant change compared to the previous setup. On the contrary: the RMSE at the control points, first of all the Z-component, increases. The speculation is that the given calibration parameters are not optimal. Therefore, in the last setup, also the IO and distortion parameters for the vertical camera are estimated within the adjustment. Now, compared to the previous setup, the RMSE at the Z-component of the control points decrease again, but is not as good as in the second setup, where only the oblique images were used. However, the RMSE at most scene constraints and check features decrease, also compared to the only-oblique case.

Comparing the results from the four tested approaches, some interesting observations can be made. Boujou seems not to be suited perfectly for this dataset, most probably because it might have problems if less than 4 GCPs are available for the initial parame-

ter estimation. The scene constraint *vertical line* had no impact on the results. Moreover, the fact that the radial distortion is not estimated per camera device, but globally leads to additional inaccuracies. This problem is not observable for ImageModeler, and also the incorporation of GCPs is more flexible in that software. The results from ImageModeler and our approach are comparable, but the explicit use of scene constraints in our approach leads to smaller RMSE at those features, whereas the RMSE at control points are larger in our solution. This is because in ImageModeler the reprojection error at the GCPs is minimized and only the right angle constraint is considered, whereas our algorithm needs to balance between all possible external constraints, which might contain some tension. A similar observation as for ImageModeler can be made for LPS. The errors at GCPs are even smaller than in ImageModeler, but the other measures show bigger differences. Looking at the residuals at check points it can be seen that the ITC approach resulted in the least error. This may allow to conclude that the overall scene geometry gets enhanced by the constraints.

3.3 Free net adjustment, incorporating scene constraints

In a last experiment our approach was applied in a free net adjustment. The idea is to simulate the case where no GCP information is available, thus no datum information can be used to fix the absolute orientation of the block. The advantage of incorporating scene constraints is that the block can be aligned according to buildings existing in the scene and to further support the overall geometry, as sketched in Fig. 1. For these experiments we only computed a reference distance from two GCPs and incorporated it as *known distance* into the adjustment. To remove the remaining rank defect (6 dof), approximated coordinates of 2 arbitrarily chosen tie points were fixed. The accuracy is checked using reference distances between the GCPs. Since the self-calibration of the intrinsic parameters can be based solely on the image information and intersection geometry, we also apply self-calibration in the following. All images from the above experiment are used and two different setups were defined: self-calibration without constraints (`I`) and self-calibration with constraints (`II`). From the results shown in Table 2 it is quite obvious that without employing the scene constraints the block is not aligned adequately to the actual building geometry, because of the errors in the approximate values. The scene checks and constraints in the second setup show that the block is nicely fitting to the constraints as defined at buildings. Similar to the findings from the previous experiments it can be observed that the residuals at the control information are larger if scene constraints are actively used. The same explanation as above applies here namely that tensions being present in the configuration are distributed amongst all the control constraints. However, no hint can be found from these experiments that the overall scene geometry is improved as the RMSE at the right-angle check only decreases marginally.

Assessment	I	II
Res. at control distance	0.023	0.053
Res. at check distance	0.159	0.154
Res. at H-constraints	–	0.024
Res. at H-check	2.869	0.114
Res. at V-constraints	–	0.051
Res. at V-check	2.539	0.044
Res. at RA-constraints	–	0.013
Res. at RA-check	3.882	3.697

Table 2: Results from free net adjustment

4 CONCLUSIONS

In this paper we describe our approach to the explicit incorporation of so-called scene constraints into the bundle adjustment of oblique and vertical airborne images. Scene constraints are defined at building façades and the motivation for this incorporation is mainly to stabilize the whole block. In the case of free bundle adjustment the idea is to support the alignment of the scene in accordance to the buildings in the scene. Our approach was compared to commercial software solutions from different domains. The experiments revealed that the use of the constraints actually supports the stability of the overall geometry. In addition, the possibility to calibrate all devices of a multi-device project simultaneously showed advantages over the commercial solutions. Such a multi-device calibration is also possible in the tested ImageModeler, but this software does not allow the definition of horizontal or vertical lines. Thus, the overall performance of our method for the tested dataset was slightly better. Another finding is that the flexible usage of ground control information, e.g. only the use of height control or known distance helps to increase the overall quality. Only LPS and our own approach allow to use such information.

REFERENCES

Früh, C., Sammon, R. and Zakhor, A., 2004. Automated texture mapping of 3d city models with oblique aerial imagery. In: 3D Data Processing Visualization and Transmission, International Symposium on, pp. 396–403.

Gerke, M., 2008. Dense image matching in airborne video sequences. In: ISPRS: XXI congress : Silk road for information from imagery, Vol. XXXVII-B3b, International Archives of Photogrammetry and Remote Sensing, Beijing, pp. 639–644.

Grenzdörffer, G. J., Guretzki, M. and Friedlander, I., 2008. Photogrammetric image acquisition and image analysis of oblique imagery. The Photogrammetric Record 23(124), pp. 372–386.

Höhle, J., 2008. Photogrammetric measurements in oblique aerial images. Photogrammetrie Fernerkundung Geoinformation 1, pp. 7–14.

Kurz, F., Müller, R., Stephani, M., Reinartz, P. and Schröder, M., 2007. Calibration of a wide-angle digital camera system for near real time scenarios. In: High-Resolution Earth Imaging for Geospatial Information, Vol. 36, International Archives of Photogrammetry and Remote Sensing, Hannover.

Lemmen, M., Lemmen, C. and Wubbe, M., 2007. Pictometry : potentials for land administration. In: Proceedings of the 6th FIG regional conference, International Federation of Surveyors (FIG).

Luhmann, T., Robson, S., Kyle, S. and Harley, I., 2006. Close range photogrammetry : principles, techniques and applications. Whittles, Caithness.

Mishra, P., Ofek, E. and Kimchi, G., 2008. Validation of vector data using oblique images. In: Proceedings of the 16th ACM SIGSPATIAL International conference on advances in Geographic Information Systems, ACM, Irvine, California.

Niemeier, W., 2002. Ausgleichungsrechnung. Eine Einführung für Studierende und Praktiker des Vermessungs- und Geoinformationswesens. de Gruyter, Berlin.

Petrie, G. and Walker, A. S., 2007. Airborne digital imaging technology: a new overview. The Photogrammetric Record 22(119), pp. 203–225.

Wang, M., Bai, H. and Hu, F., 2008. Automatic texture acquisition for 3d model using oblique aerial images. In: Intelligent Networks and Intelligent Systems, International Workshop on, pp. 495–498.